Author's Accepted Manuscript

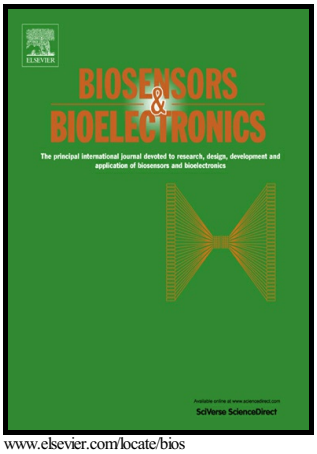

www.elsevier.com/locate/bios

A highly sensitive impedimetric aptasensor for the selective detection of acetamiprid and atrazine based on microwires formed by platinum nanoparticles

L. Madianos, G. Tsekenis, E. Skotadis, L. Patsiouras, D. Tsoukalas

PII: S0956-5663(17)30700-5
DOI: https://doi.org/10.1016/j.bios.2017.10.034
Reference: BIOS10059

To appear in: *Biosensors and Bioelectronic*

Received date: 24 July 2017
Revised date: 26 September 2017
Accepted date: 15 October 2017

Cite this article as: L. Madianos, G. Tsekenis, E. Skotadis, L. Patsiouras and D. Tsoukalas, A highly sensitive impedimetric aptasensor for the selective detection of acetamiprid and atrazine based on microwires formed by platinum nanoparticles, *Biosensors and Bioelectronic,* https://doi.org/10.1016/j.bios.2017.10.034

A highly sensitive impedimetric aptasensor for the selective detection of acetamiprid and atrazine based on microwires formed by platinum nanoparticles

L. Madianos[a], G. Tsekenis[b], E. Skotadis[a], L. Patsiouras[a], D. Tsoukalas[a*]

[a] Department of Applied Physics, National Technical University of Athens, Athens, 15780, Greece

[b] Biomedical Research Foundation of the Academy of Athens, Athens, 11527, Greece

*Corresponding authors e-mails: madleo@mail.ntua.com, dtsouk@central.ntua.gr, tel:

+30 2107721679

Department of Applied Physics, National Technical University of Athens, Iroon Polytexneiou 9, 15780, Greece

Abstract

A novel impedimetric biosensor was developed for the detection of the two extensively used pesticides, acetamiprid and atrazine. By employing the sputtering and e-beam lithography techniques, platinum nanoparticles (Pt NPs) were deposited in a bridge-like arrangement, in between interdigitated electrodes (IDEs). The resulting Pt NP microwires were chemically functionalized to allow the covalent immobilization of aptamers against the two target analytes onto the sensor surfaces. The biosensing platform facilitated charge transfer through the microwire-bridged IDEs, while upon analyte binding to the immobilized aptamers electron transfer was hindered, resulting in an increase of the electrochemical cell's impedance. The combination of Pt NPs microwires and aptamers allowed the sensitive and highly selective detection of acetamiprid with a linear range of response in the range of 10 pM to 100 nM with a limit of detection (LoD) at 1 pM, and of atrazine with a linear range of responses from 100 pM to 1 μM and a LoD at 10 pM respectively. Its performance was tested against a number of other commonly used pesticides as well as in real water samples.

Keywords

platinum nanoparticles; microwires; aptamer; pesticides; impedance; biosensor; electrochemical

1. Introduction

In the past decades, pesticides have been widely employed to increase crop yields and improve the quality of agricultural products. These compounds, albeit indispensable in the modern agricultural field, are also a major source of contamination of the natural environment, with serious health concerns associated with their use (Carter and Blizard, 2016; Fratrić et al., 2017; Metayer et al., 2016). Two of the most

extensively employed such substances are atrazine and acetamiprid. The former has been banned by the European Union since 2004 (Sass and Colangelo, 2006) as it is suspected to disrupt the endocrine system (Albanito et al., 2008) and has been associated with carcinogenesis (Tchounwou et al., 2001) and birth defects (Cooper et al., 2007). The widespread use of acetamiprid, on the other hand, may pose a potential health risk to human beings exposed either to its metabolism by-products (Marfo et al., 2015) or to adjuvants commonly added to the insecticide (Mesnage et al., 2014), despite the lack of evidence as to its carcinogenicity, neurotoxicity or mutagenicity. A recent study has implicated acetamiprid in erectile dysfunction in human males (Kaur et al., 2015). Therefore, frequent use of both pesticides is a cause of concern for the public health and there is a real need to develop reliable, low-cost and easy-to-use on site methods for their detection. The gold standard for the detection of these pesticides are analytical techniques such as gas chromatography, high performance liquid chromatography (HPLC) and electrophoresis (Jia et al., 2016). These methods are very robust and well established, but lack the simplicity and cost-efficiency that a device for frequent monitoring of pesticides should possess.

In an attempt to address these issues a number of biosensors have been developed that rely on different biorecognition molecules. Most of the published work on biosensors for pesticide detection is based on antibodies, (Belkhamssa et al., 2016; Bhardwaj et al., 2015; Grennan et al., 2003). Nevertheless, and despite their advantages over traditional analytical techniques, antibody-based assays still have a number of drawbacks such as their instability and cost. (Hayat and Marty, 2014). In addition, more than one group reported on the inability of the antibody against atrazine to differentiate between closely-related molecules, thus lowering the specificity of the immunosensor. (Raman Suri et al., 2009; Williams et al., 2014) Contrary to antibodies, aptamers are nucleic acids (DNA or RNA) that can selectively bind to analytes with affinity constants comparable to those of antibodies (Hayat and Marty, 2014). Aptasensors for pesticide detection have recently gained considerable attention due to their advantages over antibodies such as low cost, low batch to batch variation and ability to be regenerated thus allowing the fabrication of reusable sensors (Sharma et al., 2015). A DNA aptamer against atrazine was selected as early as 2004 (Mulchandani, 2004), while Sanchez reported an aptamer with a different sequence (Sanchez, 2012). According to Williams et al., both of them had a low binding affinity to atrazine and this is why they selected a third DNA aptamer against this analyte (Williams et al., 2014). By contrast, only one DNA aptamer against acetamiprid has been selected by He et al. (He et al., 2011).

The aptamers against both pesticides have been used to fabricate biosensors based on a number of different transduction principles (fluorescent (Dou et al., 2015; Liu et al., 2016), colorimetric (Shi et al., 2013; Yang et al., 2014), chemiluminescent (Qi et al., 2016). Electrochemical aptasensors are by far the most researched and developed type of aptamer-based biosensor for pesticide monitoring due to their simplicity, low cost, rapid response and high sensitivity, as well as their compatibility with novel microfabrication technologies (Danesh et al., 2016; Zhou et al., 2014). However, such sensors make use of some form of labeling due to the electrochemically inert nature of the aptamer-pesticide recognition event (Li et al., 2016; Liu et al., 2016). By contrast,

Electrochemical Impedance Spectroscopy (EIS) is a highly sensitive, electrochemical method, which does not rely on the use of labels. So far, no aptasensors have been published for atrazine while three impedimetric aptasensors have been published for acetamiprid. Fei et al., proposed complex composites of Au NP decorated multiwalled carbon nanotube-reduced graphene oxide nanoribbons (Fei et al., 2015), whilst Fan et al. based their impedimetric aptasensor on the use of Au NPs modified bare Au electrodes (Fan et al., 2013). Finally, Jiang et al., based acetamiprid's detection on silver NPs anchored on nitrogen-doped graphene (Jiang et al., 2015).

Herein we present an impedimetric biosensor for the detection of atrazine and acetamiprid with high specificity, based on aptamer-modified Pt NP microwires. The sensitivity of the sensor has been improved, compared to that of conventional impedimetric sensors that employ interdigitated electrodes (IDEs), by the deposition of Pt NPs arranged to form microwires that act as bridges between the IDEs. Analyte binding to the immobilized aptamers inhibits charge transport through the microwires and as the sensors are exposed to increasing pesticide concentrations, increases in the impedance are recorded. These advancements in sensor fabrication allowed a low LoD to be achieved for both pesticides in the range of a few pM.

2. Materials and Methods

2.1. Reagents

The aptamer sequences were chosen according to prior reported literature. They were synthesized with a thiol modification at the 5'end and a Fluorescein tag at the 3' end and purchased from Aldrich Chemicals.

Acetamiprid aptamer (He et al., 2011):

5′-(SH)-$(CH_2)_6$-
TGTAATTTGTCTGCAGCGGTTCTTGATCGCTGACACCATATTATGAAGA-
[Flc]-3'

Atrazine aptamer (Williams et al., 2014):

5′-(SH)-$(CH_2)_6$-TACTGTTTGCACTGGCGGATTTAGCCAGTCAGTG-[Flc]-3'

All other reagents, including acetamiprid and atrazine, were obtained from Aldrich Chemicals. All solutions were prepared with deionized water (18 MΩ/cm resistivity) from a Millipore MilliQ system. Aptamer stock solutions were prepared in Tris–EDTA buffer (TE, pH 8.0) and kept frozen. Aptamer working solutions of different concentrations were prepared with 50 mM Tris–HCl buffer (pH 7.4, containing 0.1 M NaCl, 0.2 M KCl, 5.0 mM $MgCl_2$) (Buffer 1). 0.1 M phosphate buffer (PBS, pH 7.0) containing 5 mM $K_3[Fe(CN)_6]/K_4[Fe(CN)_6]$ (1:1, v/v) (Buffer 2) was chosen as the supporting electrolyte for the EIS measurements and the preparation of the pesticide solutions at different concentrations.

2.2. Fabrication of device

2.2.1 Fabrication of IDEs

All fabrication experiments were conducted at room temperature. Silicon wafers with a thermal oxide layer of 500 nm, were used as deposition substrates throughout the

experiments. Using conventional optical lithography, IDEs were patterned on top of the oxidized silicon substrates. By employing the e-gun evaporation technique, a Titanium layer of 3–5 nm in thickness was deposited to act as an adhesion layer between Au and the SiO_2 substrate. This was followed by Au deposition which formed electrodes with a thickness of 25 nm after lift-off. The interdigitated electrodes inter finger distance (or electrode gap) was 5 μm and 30μm, while their width was determined to be 10 μm. IDE arrays were fabricated on each square substrateTheir topology and dimensions were characterized with the use of Scanning Electron Microscope (SEM) (Figure S1).

2.2.2 Fabrication of microwires

The IDEs were covered with a Poly (methyl methacrylate) (PMMA) resist 2% (w/v) in Propylene glycol monomethyl ether acetate (PGMEA). The resist layer was formed by spin coating at 3000 rpm for 30 sec, which resulted in a mean thickness of 57 nm. The samples were baked at 160 °C for 1 and a half hours. They were subsequently exposed at a 25 kV electron beam. Electron exposure was followed by development in isopropanol/DI water solution (7:3 v/v) for 40 sec. The electron beam lithography system used was RAITH's ELPHY Quantum, installed in a Nova NanoSEM 230 Scanning Electron Microscope. Following the microwire patterning on top of PMMA's surface, Pt NPs were deposited onto the surfaces. The NP layer was fabricated by employing a DC magnetron sputtering system. Lastly, by using a lift-off process, the NPs in the unexposed area were removed, leaving only the microwires bridging the electrode gaps. The lift-off process included the immersion of the NP-coated samples in hot acetone at 45 ^{0}C for 40 min, followed by sonication for a few seconds. This resulted in the fabrication of 10 microwires made up of Pt NPs placed vertically to the IDEs. Their dimensions were 300 nm (width) x 480 μm (length) as determined with the use of SEM (Figure S2). The surface coverage of the microwires with NPs and their mean diameter (4-6 nm), both determined with the use of a Transmission Electron Microscope (TEM) (Figure S3). Atomic Force Microscopy (AFM) was used to characterize the roughness of the microwires (1.4 nm) and their height (24 nm) (Figure S4).

2.2.3. Surface functionalization and aptamer immobilization

Following fabrication of the IDEs and the formation of the microwires, the substrates were functionalized with (3-glycidyloxypropyl)triethoxysilane (GOPTS), a silane bearing epoxy moieties that allows the covalent attachment of thiol-modified aptamers, as described in (Tsekenis et al., 2012). Thiol-modified aptamers at different concentrations were incubated onto GOPTS-functionalized surfaces overnight at room temperature in Buffer 1. Upon binding, the substrates were rinsed twice with Buffer 1 and were subsequently exposed to a solution of 1 mM 6-Mercapto-1-hexanol (MCH) for 1h to remove any non-specifically bound molecules (Figure 1). Prior to EIS interrogation the surfaces were rinsed twice with Buffer 1. The amount of bound aptamer (fluorescently tagged) was quantified with the use of a Leica Confocal Microscope and ImageJ software.

2.4 Experimental measurements

EIS measurements were performed using an Agilent 4284A impedance analyzer which was connected to the IDEs through a test fixture. The analyzer was linked to a Gateway G6-350 PC and controlled by Lab View Software (GPIB). EIS measurements were recorded between 100 Hz to 1000000 Hz with a modulation voltage of 25 mV. All measurements were performed in a custom-made electrochemical cell containing 100 μL Buffer 2 and increasing concentrations of acetamiprid or atrazine for different durations of time. Following incubation with the analyte, the aptamer-functionalized surfaces were washed with Buffer 2 to remove any unbound analyte. All measurements were performed in triplicate.

3. Results and discussion

3.1 Fabrication and characterization of the sensor

Parameters such as the digit width and digit spacing are of outmost importance in electrochemical measurements, with smaller interdigit spacing generally resulting in more sensitive analyte detection (Bonanni et al., 2010). For this reason, two different digit spacing distances were tested (5 μm and 30 μm). As the spacing between the digits increased, the resulting electric field magnitude between them decreased, while the resistance increased (which coincides with the simulations of MacKay et al. (MacKay et al., 2015) (results not shown). For this reason, and in all subsequent measurements, the Au IDEs were patterned at a distance of 5 μm.

In previously published results by our research group (Skotadis et al., 2016), it has been shown that there is an optimal surface coverage with NPs, which in turn translates in a device conductivity, resistance and impedance that best serve the performance of the biosensor. In fact, optimal NP surface coverage was established to be in the range of 42%-46% (or in the range of 600 kΩ to 10 MΩ for device resistance) which is substantially close to the critical density for percolation processes in a planar surface film. Devices whose conductivity lies just below the percolation threshold present increased sensing performance. By the in-situ monitoring of the resistance of a device, the NP deposition can be interrupted just below the percolation threshold. However in order to compensate for the reduced dimensions (hence reduced number of conductive charge transport pathways) offered by the microwires, the Pt NP surface coverage had to be increased to 67%. Since the biosensors are fabricated using e-beam lithography, the 10 microwire configuration was selected to be used throughout all experiments in order to produce operational and reliable devices and at the same time to reduce the duration of the fabrication process and its respective costs.

3.2 Optimization of the biological assay

A range of concentrations of acetamiprid aptamer were deposited onto the functionalized surfaces. A peak in the fluorescence intensity was achieved at an aptamer concentration of 10 μM, while further increases in the amount of deposited aptamer did not result in any significant increase in the fluorescence (Figure S5). Increasing the aptamer surface density beyond the saturation point results in increased

steric hindrance and therefore reduced amounts of analyte binding to them (Tsekenis et al., 2012). For this reason, all subsequent experimental set-ups were performed using 10 μM of aptamer. Similar results were obtained for the aptamer against atrazine.

The effect of the incubation time on the amount of bound analyte was subsequently investigated. Once again, the aptamer against acetamiprid was chosen as a model system to measure the total impedance of the two electrode system prior to and following exposure of the aptamer-functionalized surfaces to $1x10^{-6}$ M acetamiprid in Buffer 2 for different periods of time (Figure S6). A steady increase in the percentage change in impedance with increasing incubation times can be observed, reaching a plateau at 60 minutes. The relatively slow kinetics observed can be attributed to the slow delivery of target molecules to the sensor surfaces and are limited by mass transport phenomena such as convection and diffusion (Squires et al., 2008), especially so in our custom-made electrochemical cell with its relatively large dimensions.

3.3 Detection of acetamiprid and atrazine with high sensitivity

Under the optimal experimental conditions, the EIS responses of both the unmodified IDEs as well as microwire-modified IDEs upon incubation with acetamiprid (both of them at a concentration of 10^{-6} M in Buffer 2) were obtained (Figure 2). The Bode plots of total impedance and phase angle at a range of frequencies display similar behavior for both pesticides. Total impedance Z was calculated using the following formula:

$$|Z| = (R^2+X^2)^{0.5}$$

, where R is the real part of impedance, while X refers to the imaginary part. The phase angle θ is equal to $\theta = \arctan(X/R)$ and determines how much the current will lead or lag the voltage waveform in a reactive circuit. The recorded impedance can be analyzed by fitting to an equivalent electrical circuit model. It consists of an active electrolyte resistance R_S in series with the parallel combination of the double-layer capacitance C_{dl} and an impedance of a faradaic reaction (charge transfer resistance (Rct) and warburg impedance (Zw). In the case of the microwire-modified sensors, their resistance Rm/w should be added in parallel to the electrolyte resistance Rs to better describe the phenomena that occur on the surface of the sensors (Randles equivalent circuits provided in the inset of Figure 2B). At higher frequencies ($>10^4$ Hz), the recorded impedance is solely due to the electrolyte resistance that remains constant irrespectively of the surface modifications or the presence of the targeted analyte and corresponds to the horizontal line that can be seen in all of the Bode plots in Figure 2. At lower frequencies ($<10^3$ Hz), a capacitive behavior can be discerned which differs between the microwire functionalized IDEs (Figures 2B and 2D) and the bare ones (Figures 2A and 2C). The observed slope is characteristic of the double layer capacitance at the electrode interface caused by the absorption of ions/molecules from the medium onto the surface of the electrodes. At intermediate frequencies (10^3-10^4 Hz) both the double layer capacitance and the electrolyte resistance contribute to the impedance and this is why the percentage difference in impedance prior to and

upon exposure to analyte was calculated at 10^3 Hz, where the largest changes were recorded.

For the microwire-functionalized IDEs the total impedance was lower than that of the bare electrodes, which is due to the path through which electrons can flow in between the Au IDEs. In the case of the microwire-functionalized IDE arrays, exposure to the analyte results in a significant increase in the total impedance of the system, while in their absence the analyte does not have a significant effect on the total impedance. This indicates that charge transfer in the absence of microwires is already hindered by the electrode configuration, while for the microwire-functionalized IDEs, the bound analyte presents an obstacle to electron flow and has a sizeable impact on the system's resistance. Interestingly, the Nyquist plots in Figure S7 and Figure S8 further illustrate the fact that there are limited pathways through which electrons can flow between the IDEs due to the optimized Pt NP density in the microwires, which results in a lack of semicircular portions at the high frequency region. This allows the detection of the target analyte even at extremely low concentrations, since its presence has a significant effect on the system's Rct. In the opposite case, analyte binding to the immobilized aptamers would not be detected. Increasing the concentration of both analytes resulted in increased Rct as it can be seen in the inset of Figure S7 for acetamiprid and Figure S8 for atrazine.

All subsequent measurements, therefore, were carried out at the optimized conditions and on Pt NP microwire-functionalized IDE arrays. The EIS responses in Figure 3A correspond to the total impedance measured upon exposure to increasing concentrations of acetamiprid, while in Figure 3B the equivalent Bode plots for atrazine can be found (Only the total impedances at frequencies ranging between 10^2 and 10^4 Hz are plotted). In both cases, increasing concentrations of the target analyte result in increases in the total impedance, due to increases in the circuit's Rct. Calibration curves were drafted by plotting the percentage change in total impedance from the baseline (absence of analyte) for each concentration of analyte at a frequency equal to 1 kHz (Figure 3C for acetamiprid and Figure 3D for atrazine). For acetamiprid, a linear relationship between deltaZ/Z and the logarithm of analyte concentration was obtained in the range of 10 pM to 100 nM with a limit of detection (LoD) at 1 pM. For atrazine, a wide linear response from 100 pM to 1 μM was established with a limit LoD at 10 pM.The percentage difference in the system's total impedance from the baseline is significantly higher for the acetamiprid aptasensor reaching 160% upon saturation of the immobilized aptamers with their target analyte, while in the case of atrazine it averages 110% upon saturation. The differences in the recorded change in impedance as well as in the LoD can be attributed to the different dynamic shapes of the aptamers on the surfaces, especially upon recognition of their target analyte. A bulkier 3D aptamer configuration will result in less analyte being bound on the surface, taking into consideration that both pesticides are of similar size (Ilgu and Nilsen-Hamilton, 2016).

The analytical performance of the fabricated aptasensors compares favorably with published work on biosensors for the detection of these two pesticides (Table 1) As far as acetamiprid is concerned, a lower detection limit has been achieved by two research groups, albeit with the use of graphene (Jiang et al., 2015) or multiwalled

carbon nanotubes (Fei et al., 2015) in conjunction with NPs, which apart from the complexity, results in an increased cost when compared to the fabricated biosensing platform. On the other hand atrazine's detection, up until now has only been realized with the use of immunoassays, while the proposed biosensing platform is the only aptamer-based protocol, which at the same time achieves the lowest LoD (Table 1).

3.4 Selectivity of the pesticide aptasensors

The presence of pesticides in real samples, other than the ones targeted by the fabricated biosensors, and their non-specific interaction with the immobilized aptamers could lead to erroneous measurements. The selectivity of the two sensing platforms was therefore tested against acetamiprid and atrazine respectively, in the presence of one another as well as two other pesticides, chlorpyrifos and carbaryl. The sensors functionalized with the aptamer against acetamiprid were able to selectively recognize acetamiprid, their mean response exceeding the response recorded for the other three pesticides by a factor of 8 (Figure 4A). The mean response obtained from the sensors functionalized with the aptamer against atrazine upon incubation with their target analyte was again greater than the non-specific signal by a factor of 5 (Figure 4B).

3.5 Pesticide detection in real samples

In order to validate the feasibility of the method to analyze these two pesticides, the performance of the biosensing platform was evaluated with two real samples, tap water and bottled mineral water. Control experiments were undertaken by spiking the samples with known concentrations of the two pesticides (n=5 for each concentration of pesticide) without pre-treatment or clean up steps, in order to evaluate the occurrence of matrix effects (5 mM $K_3[Fe(CN)_6]/K_4[Fe(CN)_6]$ (1:1, v/v) were added to the water samples prior to analysis). The results showed excellent spiked recoveries in the range of 79~113% from all the water samples for the two pesticides (Table 2). Lower recovery values were obtained for the tap water compared to the bottled mineral water, probably due to its high total hardness.

4. Conclusions

In summary, a simple and label-free microwire-modified aptasensor based on EIS has been developed for the detection of acetamiprid and atrazine. The optimized Pt NPs surface coverage and their arrangement in microwires allowed the determination of the two pesticides with satisfactory selectivity, reproducibility and accuracy. The recovery rates achieved with real samples pave the way for the exploitation of the proposed biosensor without the need of any sample pretreatment. This is especially so the case for EIS-based biosensors that can be easily integrated into portable devices. The analytical performance achieved solely with the use of Pt NPs compares favorably with other biosensing platforms that achieve a lower LoD for acetamiprid, albeit with the use of more than one nanomaterial. Moreover, further engineering of the biological assay could enhance the sensor's sensitivity. As an example, we have already shown that the introduction of a short complementary strand that can dissociate from the immobilized aptamer upon analyte presentation considerably

increases the response of the biosensor (Tsekenis et al., 2016). As far as the detection of atrazine is concerned, the proposed impedimetric biosensor not only achieves the lowest LoD, but most importantly is the only one to rely on the use of aptamers, which are considerably more cost efficient than other biorecognition molecules.

Figure legends

Figure 1. Schematic representation of surface functionalization. Following fabrication of the Pt NP microwires, the surfaces are silanized with GOPTS. Thiol-modified aptamers are covalently immobilized onto the surfaces and non-specifically bound aptamers are removed following incubation with MCH.

Figure 2. Comparison of the EIS responses of sensors prior to and following incubation with acetamiprid and atrazine. Bode plots of (A) unmodified and (B) microwire-modified sensor upon incubation with 10^{-6} M acetamiprid for 1 hour. The Randles equivalent circuit is provided in the insets. The equivalent Bode plots of (C) unmodified and (D) microwire-modified sensors upon incubation with 10^{-6} M atrazine for 1 hour.

Figure 3. EIS responses of the microwire-modified IDEs at different concentrations of the two pesticides. (A) The Bode plots of sensors functionalized with 10 μM of acetamiprid aptamer upon exposure to increasing concentrations of acetamiprid (from a to i: 0, $1x10^{-12}$ M, $10x10^{-12}$ M, $100x10^{-12}$ M, $1x10^{-9}$ M, $10x10^{-9}$ M, $100x10^{-9}$ M, $1x10^{-6}$ M, $10x10^{-6}$ M) in Buffer 2. (B) The equivalent Bode plots for the sensors against atrazine. The sensors were exposed to a range of concentrations of atrazine (from a to i: 0, $10x10^{-12}$ M, $100x10^{-12}$ M, $1x10^{-9}$ M, $10x10^{-9}$ M, $100x10^{-9}$ M, $1x10^{-6}$ M, $10x10^{-6}$ M, $100x10^{-6}$ M) in Buffer 2. The calibration curves obtained for the two pesticides: (C) acetamiprid and (D) atrazine.

Figure 4. Selectivity of the assay for acetamiprid and atrazine detection onto the Pt NP microwire functionalized sensors. The mean response of 5 different sensors functionalized with the aptamer against (A) acetamiprid and (B) atrazine upon incubation with 4 different pesticides ($1x10^{-6}$ M).

Table 1. Analytical performance of different electrochemical biosensors for acetamiprid and atrazine detection.

Table 2. Analysis of real water samples spiked with different concentrations of the acetamiprid and atrazine

References

Albanito, L., Lappano, R., Madeo, A., Chimento, A., Prossnitz, E.E., Cappello, A.R., Dolce, V., Abonante, S., Pezzi, V., Maggiolini, M., 2008. Health Perspect. 116, 1648–1655. doi:10.1289/ehp.11297

Belkhamssa, N., Justino, C.I.L., Santos, P.S.M., Cardoso, S., Lopes, I., Duarte, A.C., Rocha-Santos, T., Ksibi, M., 2016. Talanta 146, 430–434. doi:10.1016/j.talanta.2015.09.015

Bhardwaj, S.K., Bhardwaj, N., Mohanta, G.C., Kumar, P., Sharma, A.L., Kim, K.H., Deep, A., 2015. ACS Appl. Mater. Interfaces 7, 26124–26130. doi:10.1021/acsami.5b07692

Bonanni, A., Fernández-Cuesta, I., Borrisé, X., Pérez-Murano, F., Alegret, S., del Valle, M., 2010. Microchim. Acta 170, 275–281. doi:10.1007/s00604-010-0358-5

Carter, C.J., Blizard, R.A., 2016. Neurochem. Int., 99, 42-51, doi:10.1016/j.neuint.2016.10.011

Cooper, R.L., Laws, S.C., Das, P.C., Narotsky, M.G., Goldman, J.M., Tyrey, E.L., Stoker, T.E., 2007. Birth Defects Res. Part B - Dev. Reprod. Toxicol. doi:10.1002/bdrb.20110

Danesh, N.M., Ramezani, M., Emrani, A.S., Abnous, K., Taghdisi, S.M., 2016. Biosens. Bioelectron. 75, 123–128. doi:10.1016/j.bios.2015.08.017

Dou, X., Chu, X., Kong, W., Luo, J., Yang, M., 2015. Anal. Chim. Acta 891, 291–297. doi:10.1016/j.aca.2015.08.012

Fan, L., Zhao, G., Shi, H., Liu, M., Li, Z., 2013. Biosens. Bioelectron. 43, 12–18. doi:10.1016/j.bios.2012.11.033

Fei, A., Liu, Q., Huan, J., Qian, J., Dong, X., Qiu, B., Mao, H., Wang, K., 2015. Biosens. Bioelectron. 70, 122–129. doi:10.1016/j.bios.2015.03.028

Figueiredo-Filho, L.C.S., Azzi, D.C., Janegitz, B.C., Fatibello-Filho, O., 2012. Electroanalysis 24, 303–308. doi:10.1002/elan.201100421

Fratrić, I., Varga, J., Vukmirović, S., Sudji, J., Živković, D., 2017. J. Pediatr. Surg. 52, 1166–1168. doi:10.1016/j.jpedsurg.2016.11.048

Grennan, K., Strachan, G., Porter, A.J., Killard, A.J., Smyth, M.R., 2003. Analytica Chimica Acta. pp. 287–298. doi:10.1016/S0003-2670(03)00942-5

Hayat, A., Marty, J.L., 2014. Front. Chem. 2 (41), 1-9. doi:10.3389/fchem.2014.00041

He, J., Liu, Y., Fan, M., Liu, X., 2011. J. Agric. Food Chem. 59, 1582–1586. doi:10.1021/jf104189g

Ilgu, M., Nilsen-Hamilton, M., 2016. Aptamers in analytics. Analyst 141, 1551–1568.

doi:10.1039/C5AN01824B

Jia, L., Su, M., Wu, X., Sun, H., 2016. J. Sep. Sci. 39, 4512–4519. doi:10.1002/jssc.201600883

Jiang, D., Du, X., Liu, Q., Zhou, L., Dai, L., Qian, J., Wang, K., 2015. Analyst 140, 6404–6411. doi:10.1039/c5an01084e

Kaur, R.P., Gupta, V., Christopher, A.F., Bansal, P., 2015. Asian Pacific J. Reprod. doi:10.1016/j.apjr.2015.07.012

Li, H., Qiao, Y., Li, J., Fang, H., Fan, D., Wang, W., 2016. Biosens. Bioelectron. 77, 378–384. doi:10.1016/j.bios.2015.09.066

Liu, Q., Huan, J., Dong, X., Qian, J., Hao, N., You, T., Mao, H., Wang, K., 2016. Sensors Actuators, B Chem. 235, 647–654. doi:10.1016/j.snb.2016.05.154

MacKay, S., Hermansen, P., Wishart, D., Chen, J., 2015. Sensors (Switzerland) 15, 22192–22208. doi:10.3390/s150922192

Marfo, J.T., Fujioka, K., Ikenaka, Y., Nakayama, S.M.M., Mizukawa, H., Aoyama, Y., Ishizuka, M., Taira, K., 2015. PLoS One 10. doi:10.1371/journal.pone.0142172

Mesnage, R., Defarge, N., Spiroux De Vendômois, J., Séralini, G.E., 2014. Biomed Res. Int. 2014. doi:10.1155/2014/179691

Metayer, C., Dahl, G., Wiemels, J., Miller, M., 2016. Pediatrics 138, S45–S55. doi:10.1542/peds.2015-4268H

Mulchandani, A., 2004. Rep. - Univ. Calif. Water Resour. Cent. 69–70.

Norouzi, P., Larijani, B., Ganjali, M.R., Faridbod, F., 2012. Int. J. Electrochem. Sci. 7, 10414–10426.

Qi, Y., Xiu, F.R., Zheng, M., Li, B., 2016. Biosens. Bioelectron. 83, 243–249. doi:10.1016/j.bios.2016.04.074

Raman Suri, C., Boro, R., Nangia, Y., Gandhi, S., Sharma, P., Wangoo, N., Rajesh, K., Shekhawat, G.S., 2009. TrAC - Trends Anal. Chem. 28, 29–39. doi:10.1016/j.trac.2008.09.017

Sanchez, P.E., 2012. DNA Aptamer Development for Detection of Atrazine and Protective Antigen Toxin Using Fluorescence Polarization.

Sass, J.B., Colangelo, A., 2006. European Union bans atrazine, while the United States negotiates continued use. Int. J. Occup. Environ. Health. doi:10.1179/oeh.2006.12.3.260

Sharma, R., Ragavan, K. V., Thakur, M.S., Raghavarao, K.S.M.S., 2015. Biosens. Bioelectron. doi:10.1016/j.bios.2015.07.017

Shi, H., Zhao, G., Liu, M., Fan, L., Cao, T., 2013. J. Hazard. Mater. 260, 754–761. doi:10.1016/j.jhazmat.2013.06.031

Skotadis, E., Voutyras, K., Chatzipetrou, M., Tsekenis, G., Patsiouras, L., Madianos, L., Chatzandroulis, S., Zergioti, I., Tsoukalas, D., 2016. Biosens. Bioelectron.

81, 388–394. doi:10.1016/j.bios.2016.03.028

Squires, T.M., Messinger, R.J., Manalis, S.R., 2008. Nat. Biotechnol. 26, 417–426. doi:10.1038/nbt1388

Taghdisi, S.M., Danesh, N.M., Ramezani, M., Abnous, K., 2017. Microchim. Acta 184, 499–505. doi:10.1007/s00604-016-2038-6

Tchounwou, P.B., Wilson, B.A., Ishaque, A.B., Schneider, J., 2001. Mol. Cell. Biochem. 222, 49–59. doi:10.1023/A:1017903005541

Tsekenis, G., Chatzipetrou, M., Tanner, J., Chatzandroulis, S., Thanos, D., Tsoukalas, D., Zergioti, I., 2012. Sensors Actuators, B Chem. 175, 123–131. doi:10.1016/j.snb.2012.01.005

Tsekenis, G., Theodorakos, I., Massaouti, M., Zergioti, I., 2016. pp. 90–94. doi:10.3233/978-1-61499-653-8-90

Williams, R.M., Crihfield, C.L., Gattu, S., Holland, L.A., Sooter, L.J., 2014. Int. J. Mol. Sci. 15, 14332–14347. doi:10.3390/ijms150814332

Yang, Z., Qian, J., Yang, X., Jiang, D., Du, X., Wang, K., Mao, H., Wang, K., 2014. Biosens. Bioelectron. 65, 39–46. doi:10.1016/j.bios.2014.10.004

Yang, M., Zhao, X., Zheng, S., Liu, X., Jin, B., Li, H., Gan, Y., 2017. J. Electroanal. Chem. 791, 17–22. doi:10.1016/j.jelechem.2017.03.009

Zacco, E., Galve, R., Marco, M.P., Alegret, S., Pividori, M.I., 2007. Biosens. Bioelectron. 22, 1707–1715. doi:10.1016/j.bios.2006.07.037

Zhou, L., Wang, J., Li, D., Li, Y., 2014. Food Chem. 162, 34–40. doi:10.1016/j.foodchem.2014.04.058

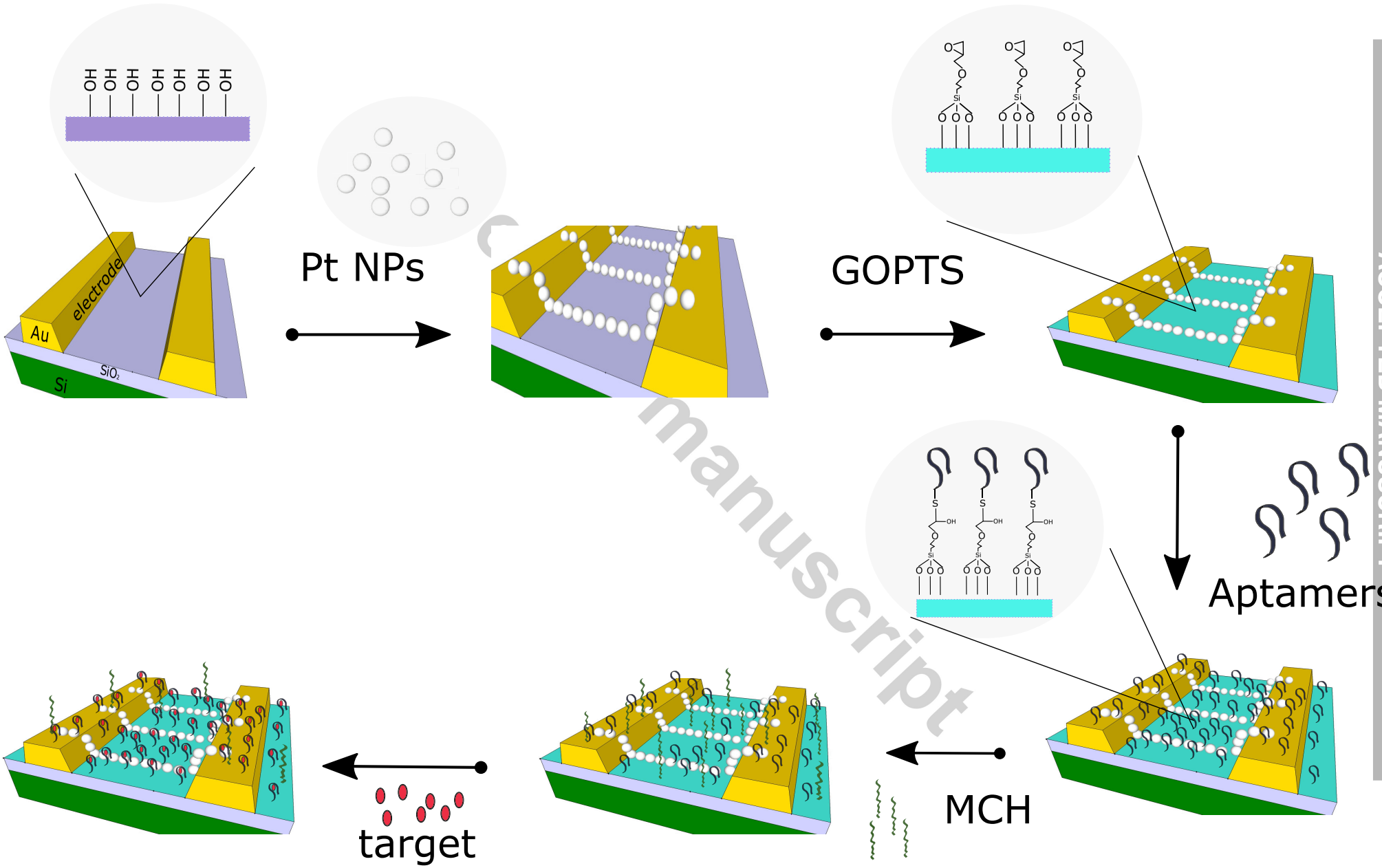

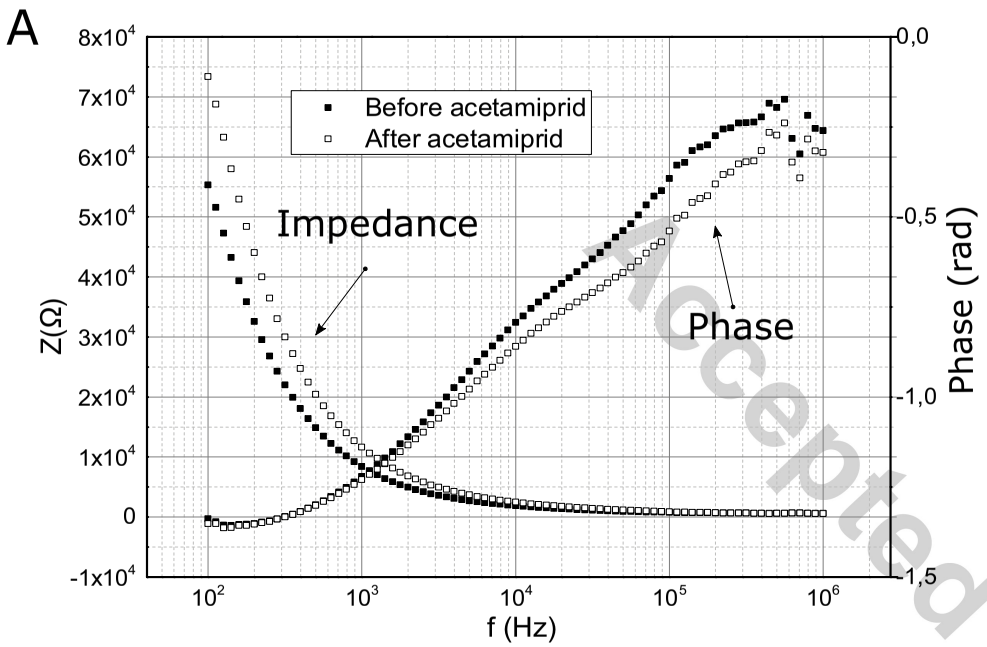

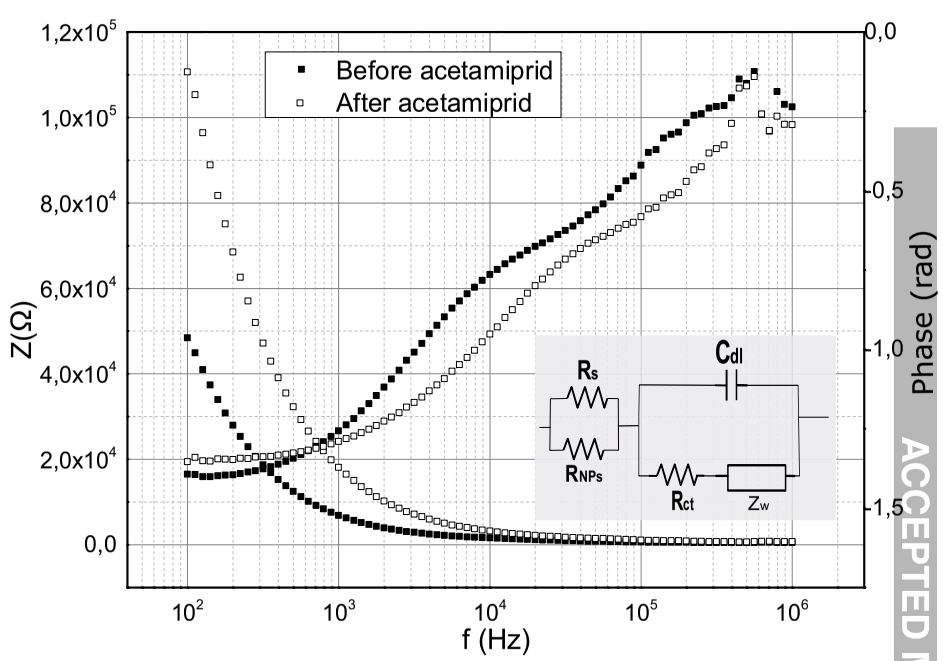

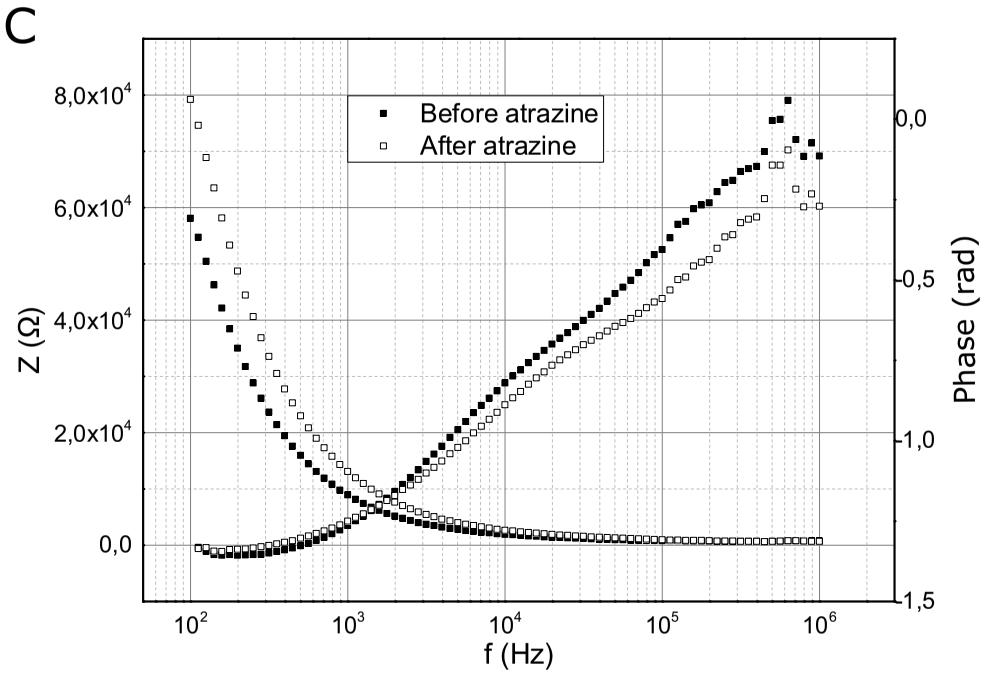

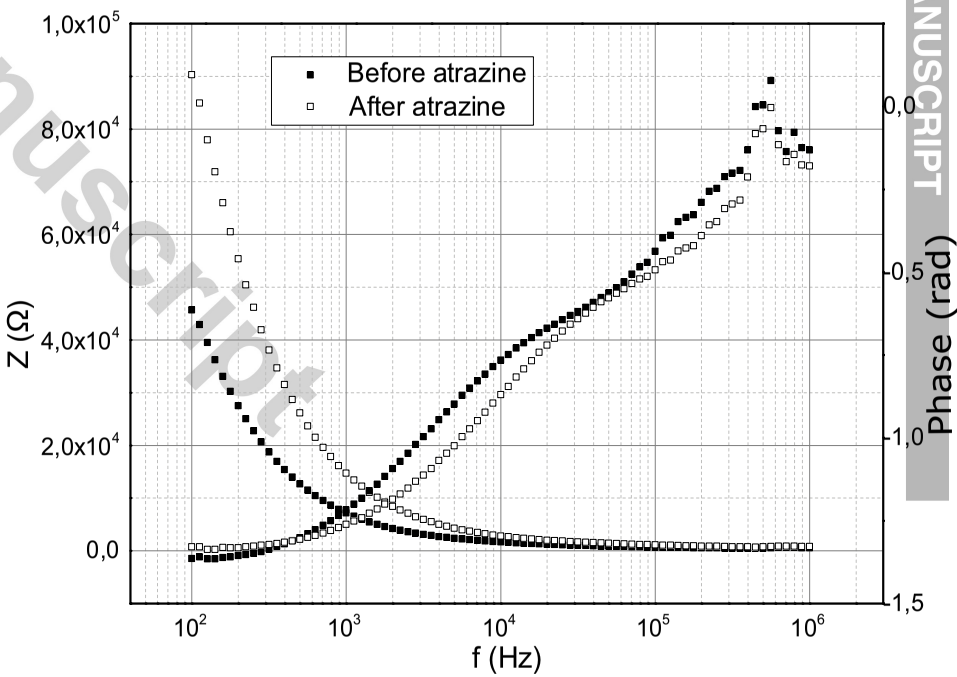

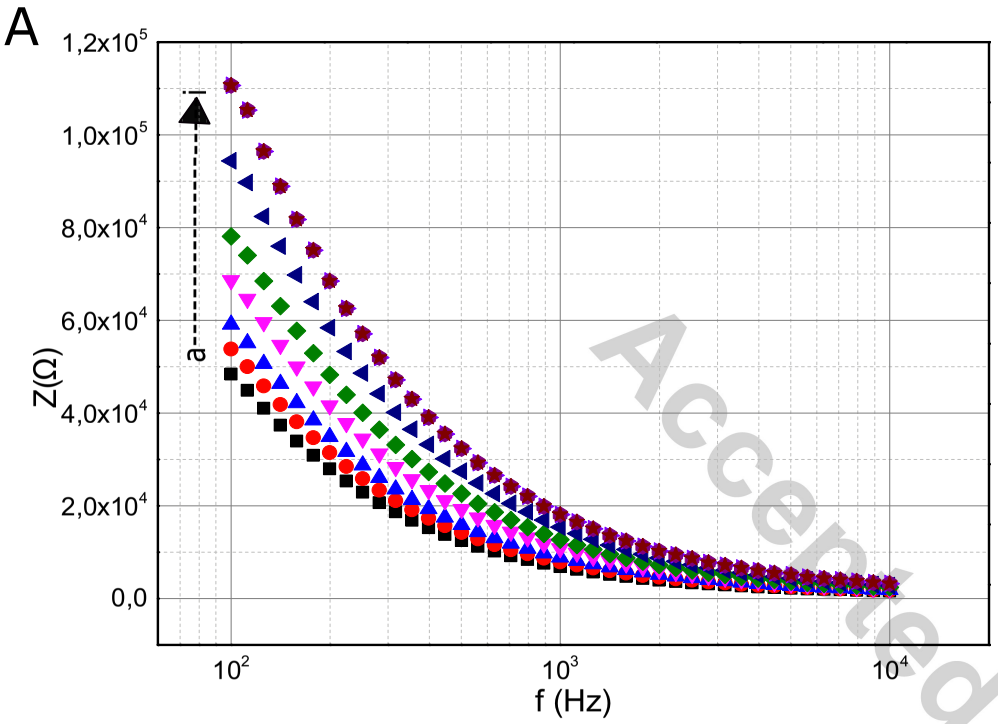

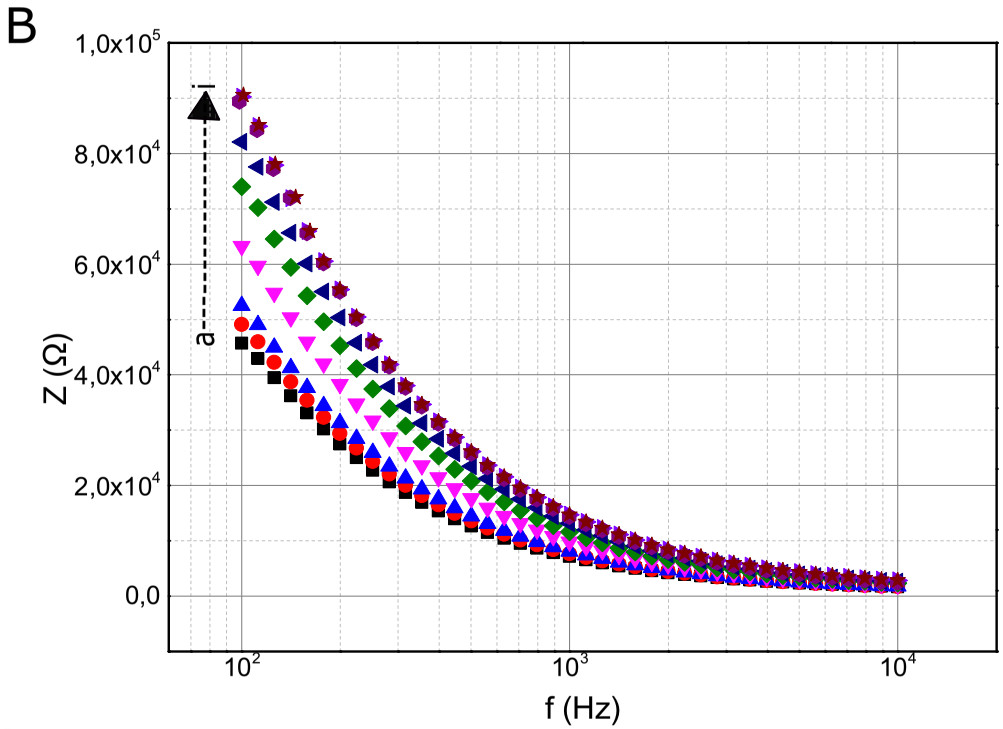

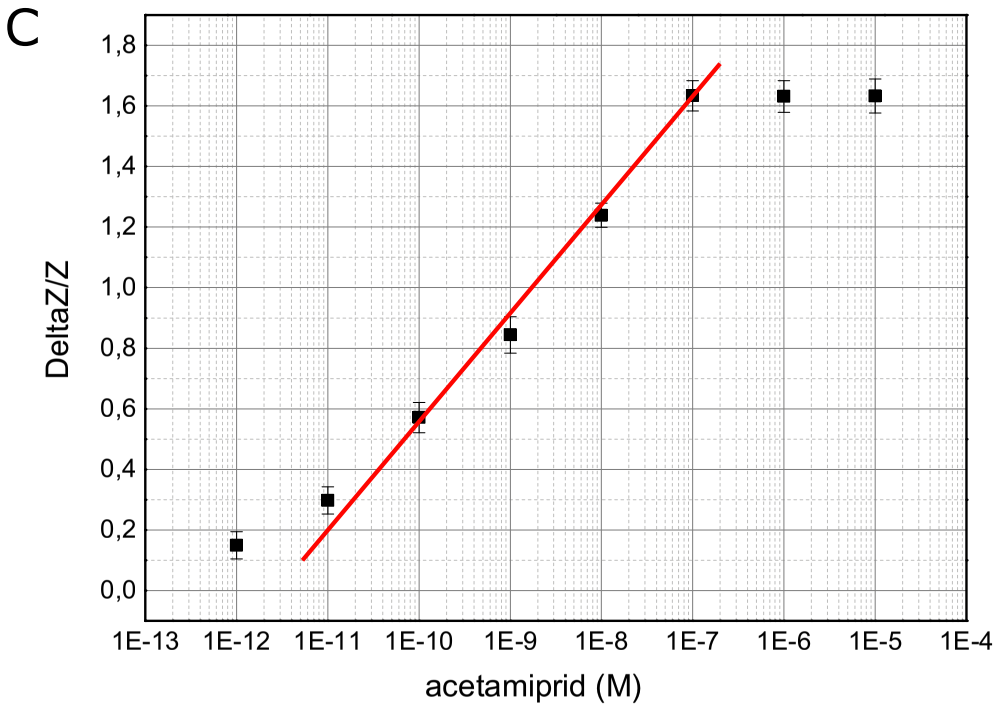

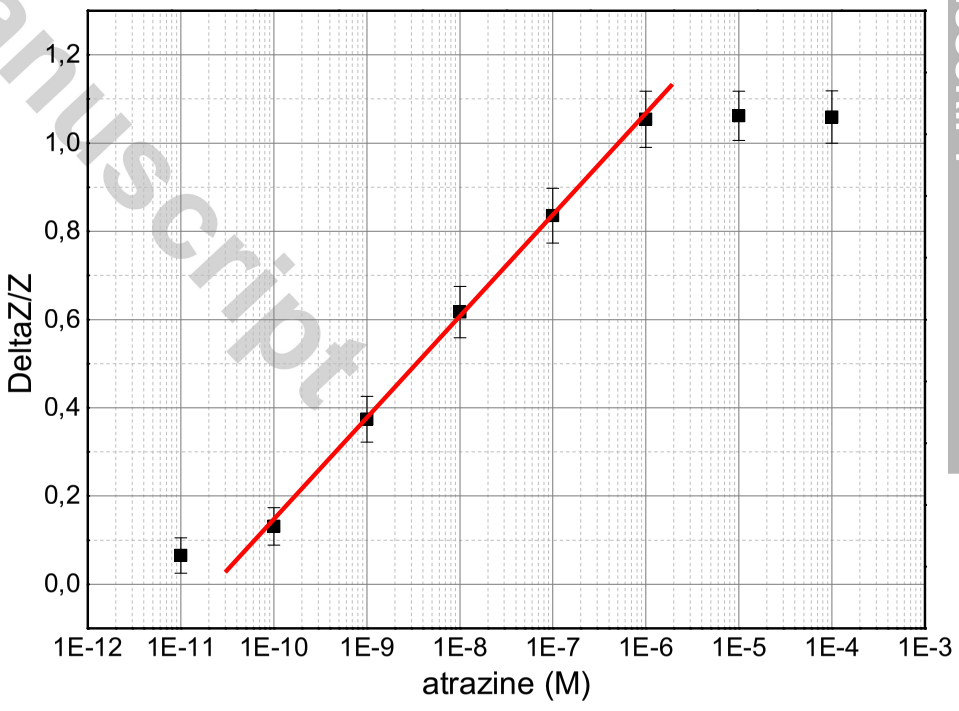

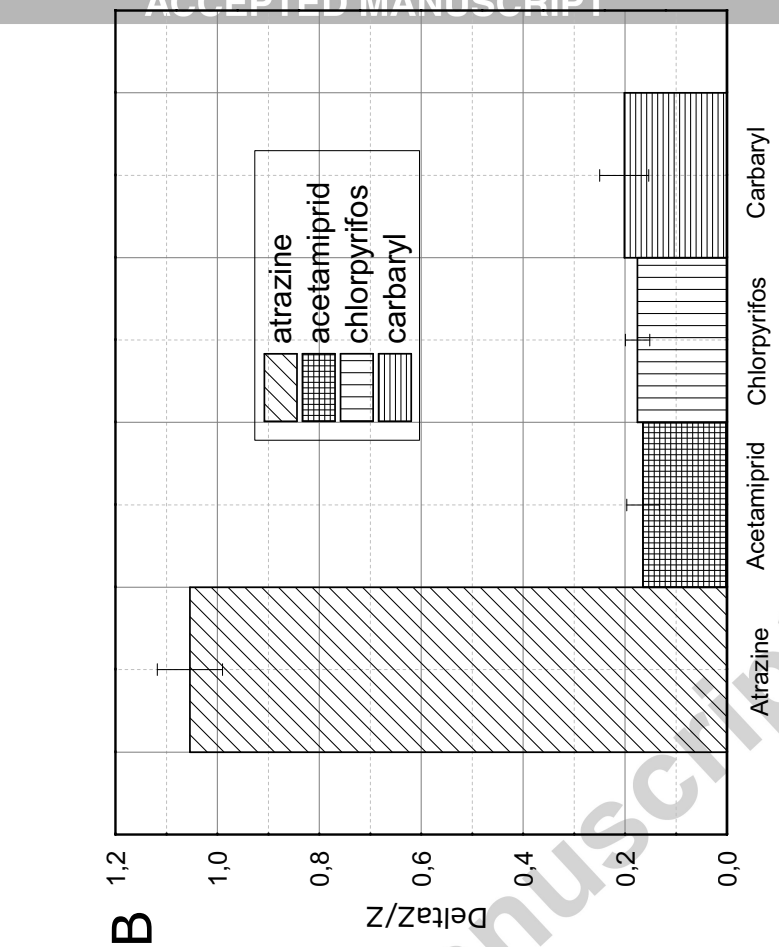

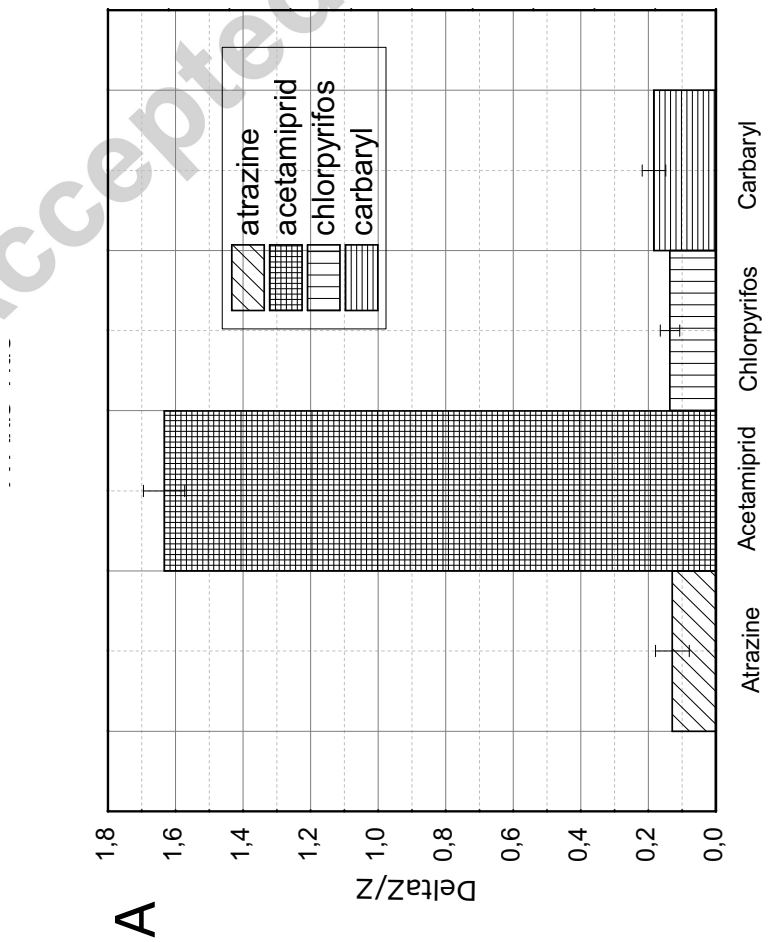

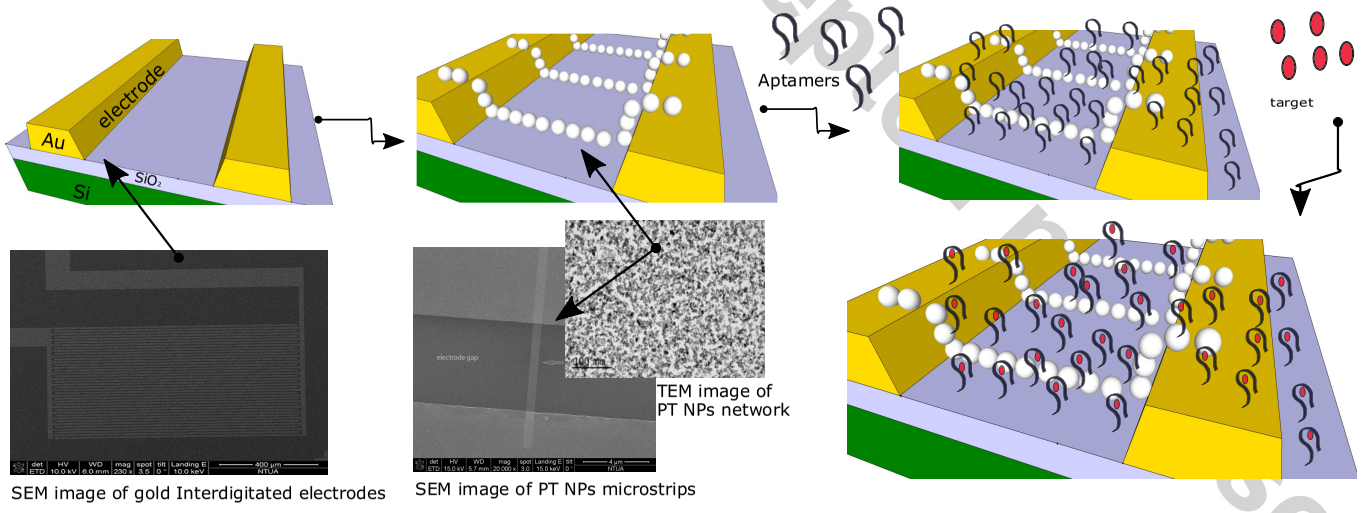

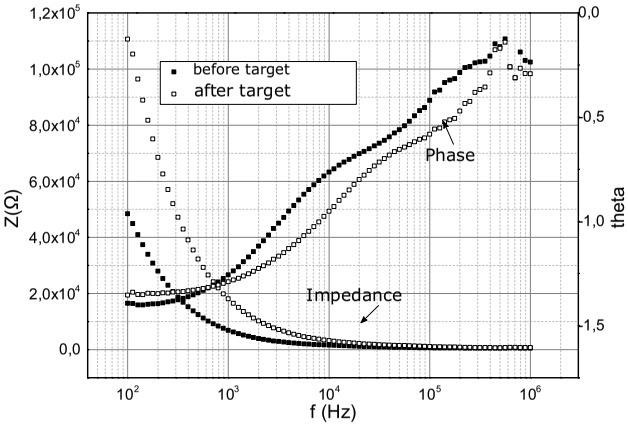

Table 1. Analytical performance of different electrochechemical biosensors for acetamiprid and atrazine detection.

	Method	Bio-recognition molecule	Strategy	Linear range (M)	Detection limit (M)	References
Acetamiprid	PEC[a]	Aptamer	Resonance energy transfer from CdTe quantum dots to Au nanorods	$0.5x10^{-12}$ - $1x10^{-5}$	$0.2x10^{-12}$	(Liu et al., 2016)
	DPV[b]	Aptamer	SiNP-streptavidin conjugate modified MB-dsDNA[d]	$0.5x10^{-9}$ - $6.5x10^{-6}$	$1.5x10^{-10}$	(Taghdisi et al., 2017)
	EIS	Aptamer	AuNPs modified electrode	5×10^{-9}- 6×10^{-7}	1×10^{-9}	(Fan et al., 2013)
	EIS	Aptamer	Au/MWCNT-rGONR[e] composites modified electrode	5×10^{-14} - 1×10^{-5}	1.7×10^{-14}	(Fei et al., 2015)
	EIS	Aptamer	Ag NPs anchored on nitrogen-doped graphene	$1x10^{-13}$ - $5x10^{-9}$	3.3×10^{-14}	(Jiang et al., 2015)
	EIS	Aptamer	PtNPs microstrips modified Au IDEs	$1x10^{-11}$ - $1x10^{-7}$	$1x10^{-12}$	This work
Atrazine	DPV	Antibody	Bismuth film electrode	6.7×10^{-7} - 2.0×10^{-5}	1.4×10^{-7}	(Figueiredo-Filho et al., 2012)
	FFT-SWV[c]	Antibody	Au/MWCNT	5×10^{-10} - $1x10^{-7}$	2×10^{-11}	(Norouzi et al., 2012)
	DPV	Antibody	Self-ordered Nb_2O_5 nanotube arrays modified with chitosan and carboxyl-Fe3O4 NPs	$1.8x10^{-10}$ - $2.7x10^{-9}$	0.8×10^{-10}	(Yang et al., 2017)
	Amperometry	Antibody	Protein A (2%) graphite–epoxy biocomposite along with atrazine-HRP tracer as the enzymatic label	$8x10^{-11}$ - $6x10^{-9}$	$3x10^{-11}$	(Zacco et al., 2007)
	EIS	Aptamer	PtNPs microstrips modified Au IDEs	$1x10^{-10}$- $1x10^{-6}$	$1x10^{-11}$	This work

[a] Photoelectrochemical
[b] Differential pulse voltammetry
[c] Fast Fourier transform - Square wave voltammetry
[d] Silica nanoparticles/ Methylene Blue-double stranded DNA
[e] Multiwalled carbon nanotube-reduced graphene oxide nanoribbon

Table 2. Analysis of real water samples spiked with different concentrations of the acetamiprid and atrazine

Acetamiprid					
Samples	Added (nM)	Found (nM)	SD	Recovery (%)	RSD (%)
Tap water	0	Undetected			
	0.1	0.086	0.003	86	3.5
	1	0.937	0.053	94	5.7
	10	10.16	0.651	102	6.4
Dioni mineral water, Rainbow waters S.A., Greece	0	Undetected			
	0.1	0.112	0.005	112	4.5
	1	1.057	0.036	106	3.4
	10	10.9	0.487	109	4.5
Atrazine					
Samples	Added (nM)	Found (nM)	SD	Recovery (%)	RSD (%)
Tap water	0	Undetected			
	0.1	0.079	0.001	79	1.3
	1	0.914	0.049	91	5.4
	10	9.87	0.405	99	4.1
Dioni mineral water, Rainbow waters S.A., Greece	0	Undetected			
	0.1	0.106	0.003	106	2.8
	1	1.082	0.041	108	3.8
	10	11.3	0.548	113	4.8

- ✓ High sensitivity achieved with the use of microwire-bridged gaps between interdigitated electrodes.
- ✓ The microwires were made of platinum nanoparticles with optimized surface coverage and dimensions.
- ✓ Aptamer-based sensitive and specific detection of two extensively used pesticides, acetamiprid and atrazine
- ✓ The first biosensor based on aptamers for the detection of atrazine is being described.
- ✓ Measurement of spiked real water samples with the fabricated biosensor with satisfactory recovery rates and RSD values.